

Intersections of potential energy surfaces of short-lived states: The complex analogue of conical intersections

Sven Feuerbacher, Thomas Sommerfeld, and Lorenz S. Cederbaum

Citation: *The Journal of Chemical Physics* **120**, 3201 (2004); doi: 10.1063/1.1640615

View online: <http://dx.doi.org/10.1063/1.1640615>

View Table of Contents: <http://scitation.aip.org/content/aip/journal/jcp/120/7?ver=pdfcov>

Published by the [AIP Publishing](#)

Articles you may be interested in

Conical intersections and diabatic potential energy surfaces for the three lowest electronic singlet states of H_3^+
J. Chem. Phys. **141**, 204306 (2014); 10.1063/1.4901986

Photodissociation of carbon dioxide in singlet valence electronic states. I. Six multiply intersecting ab initio potential energy surfaces
J. Chem. Phys. **138**, 224106 (2013); 10.1063/1.4808369

Direct calculation of coupled diabatic potential-energy surfaces for ammonia and mapping of a four-dimensional conical intersection seam
J. Chem. Phys. **124**, 124309 (2006); 10.1063/1.2168447

Theory of the photodissociation of ozone in the Hartley continuum: Potential energy surfaces, conical intersections, and photodissociation dynamics
J. Chem. Phys. **123**, 014306 (2005); 10.1063/1.1903947

Jahn-Teller effect for short-lived states: Study of the complex potential energy surfaces
J. Chem. Phys. **121**, 5 (2004); 10.1063/1.1755651



Intersections of potential energy surfaces of short-lived states: The complex analogue of conical intersections

Sven Feuerbacher,^{a)} Thomas Sommerfeld, and Lorenz S. Cederbaum

*Theoretische Chemie, Physikalisch-Chemisches Institut, Universität Heidelberg,
Im Neuenheimer Feld 229, 69120 Heidelberg, Germany*

(Received 10 September 2003; accepted 19 November 2003)

Whereas conical intersections between potential energy surfaces of bound states are well known, the interaction of short-lived states has been investigated only rarely. Here, we present several systematically constructed model Hamiltonians to study the topology of intersecting complex potential energy surfaces describing short-lived states: We find the general phenomenon of doubly intersecting complex energy surfaces, i.e., there are two points instead of one as in the case of bound states where the potential energy surfaces coalesce. In addition, seams of intersections of the respective real and imaginary parts of the potential energy surfaces emanate from these two points. Using the Σ^* and Π^* resonance states of the chloroethene anion as a practical example, we demonstrate that our complete linear model Hamiltonian is able to reproduce all phenomena found in explicitly calculated *ab initio* complex potential energy surfaces. © 2004 American Institute of Physics. [DOI: 10.1063/1.1640615]

I. INTRODUCTION

The Born–Oppenheimer approximation^{1,2} constitutes a cornerstone of quantum chemistry by enabling one to view molecules as a set of nuclei moving on potential energy surfaces (PES) provided by the eigenstates of the electronic Hamiltonian. Intersections of PES are points where this approximation usually breaks down. The phenomena occurring in the case of intersecting PES of bound states have been studied extensively and are mostly well understood. It has been found that the shape of the PES near the intersections critically depends on the interaction of the states as a function of the nuclear coordinates. In particular, under suitable conditions a so-called *conical intersection* (CI) of the PES arises leading to strong *vibronic coupling* of the states (see, e.g., Refs. 3–5 and references therein). These CIs have wide-reaching consequences for the time development of the system, e.g., greatly influence reaction pathways or the decay of excited electronic states into lower lying electronic states by opening up radiationless pathways (for recent reviews see, e.g., Refs. 6, 7). It is thus no wonder that CIs are of still increasing interest to theoreticians as well as to experimentalists. As Yarkony puts it: “It is now appreciated that what was once viewed largely as a theoretical curiosity is an essential aspect of electronically nonadiabatic processes.”⁵

Another topic much worked on is resonance states, which play a central role in many processes in physics and chemistry. Resonances are essential in electron-molecule scattering (see, e.g., Refs. 8, 9 and references therein), but also occur, e.g., in atomic and molecular collisions (see, e.g., Ref. 10 and references therein) or in molecular photoionization.⁸ In particular, metastable electronic states of any kind, for instance of anions, can be viewed as electronic resonance states. There are basically two possibilities to de-

scribe resonance states, one by Dirac and Weisskopf,^{11,12} later adapted and extended by Feshbach and Fano,^{13,14} and another by Gamow and Siegert.^{15,16} Both approaches have in common that the energy of the resonance state is a complex quantity whose imaginary part is related to the lifetime of the metastable state.

The following questions thus arise: What happens to a conical intersection if the intersecting PES cease to describe stationary states but rather belong to electronic states with a finite lifetime, i.e., resonance states? Can intersections then exist at all? And if so, can these intersections of PES of electronically *unbound* states be described by a formalism similar to that which has been very successfully used in the case of intersecting PES of *bound* states (see, e.g., Ref. 4 and references therein)? In the light of literally hundreds of publications covering CIs of *real* PES, it is quite surprising that hardly anything has been published dealing with the problem outlined here. The main work in this field was done by Estrada *et al.*¹⁷ In addition, we mention the work of Mies,¹⁸ who performed model calculations on resonances in diatomic molecules which interact by coupling to the nonresonant scattering continuum. Hazi employed the same mechanism to interpret dissociative electron attachment to hydrogen bromide.¹⁹ Another work penned by Devdariani *et al.* deals with the spectra of the decay products occurring in atomic collisions by including the interaction of resonances with two local models.²⁰ Finally, there are two recent papers analyzing the *vibronic* resonance states which result from a conical intersection between a bound and a dissociative electronic state.^{21,22} However, apart from the paper by Estrada *et al.*,¹⁷ none of these works studied the complex PES and their intersections explicitly.

In this work we extend the model Hamiltonian presented by Estrada *et al.*¹⁷ which describes the interaction of two resonance states to a more general form. We study the effects

^{a)}Electronic mail: sven.feuerbacher@pci.uni-heidelberg.de

of different systematic extensions of the Hamiltonian on the complex potential surfaces with special regard to the intersections and their topologies. The new model Hamiltonians are still analytically solvable and the most general one presented here is shown to reproduce the phenomena found in explicitly calculated *ab initio* data for a practical example. This example is the chloroethene anion, which possesses two intersecting electronic resonance states of different symmetry.

Apart from demonstrating the applicability of our new model Hamiltonian, our example is of great interest by itself: chloroethene is the prototype molecule for dissociative electron attachment to unsaturated chlorinated compounds, leading to an organic radical and a chloride anion. A description of the intersections of the resonance states in the chloroethene anion together with molecular dynamics calculations on the complex PES would be extendible to describe many other DEA processes in unsaturated halogenated compounds such as chloro- and bromobenzene^{23,24} or the biologically relevant molecule chlorouracil.^{25,26}

In the next section we start with a short discussion of the general theory of vibronic coupling and of resonance states. The new model Hamiltonians are presented in Sec. III, where we also discuss the new phenomena which emerge from the different extensions and their influence on the topology of the intersections. This is done by showing some simple, illustrative examples. Section IV is devoted to the results of our *ab initio* calculations on the chloroethene anion and to the demonstration that our new model Hamiltonian reproduces the calculated complex PES of two resonance states quite nicely in the interaction region. We close with Sec. V, where the implications of our results are summarized.

II. GENERAL THEORY

In principle, we can make use of the work done on CIs in the case of PES of bound electronic states and modify the terms appearing there to describe metastable electronic states. To do this consistently and to clarify our notation, we briefly present here the basic concepts needed. The usual case of stationary electronic states is discussed first and then transferred to the metastable states situation.

A. Coupled PES of bound electronic states

As usual (see, for instance, Refs. 4, 27), we start with the total molecular wave function $\Psi(\mathbf{r}, \mathbf{Q})$. This function includes both nuclear and electronic motion, wherein \mathbf{Q} designates *all* nuclear coordinates and \mathbf{r} *all* electronic coordinates. The next step is to expand $\Psi(\mathbf{r}, \mathbf{Q})$ in a product of a set of electronic wave functions $\{\phi_j(\mathbf{r}; \mathbf{Q})\}$ and of a set of nuclear motion wave functions $\{\chi_j(\mathbf{Q})\}$

$$\Psi(\mathbf{r}, \mathbf{Q}) = \sum_j \phi_j(\mathbf{r}; \mathbf{Q}) \chi_j(\mathbf{Q}). \quad (1)$$

For the set $\{\phi_j(\mathbf{r}; \mathbf{Q})\}$ we choose the stationary solutions of the *electronic* Hamiltonian $\hat{H}_{el}(\mathbf{r}, \mathbf{Q})$, denoted by $\{\phi_i^{\text{ad}}\}$ (the superscript “ad” stands for adiabatic). In the following we drop the explicit dependency of ϕ_i and χ_i on the coordinates for simplicity. By inserting the ansatz (1) into the mo-

lecular Schrödinger equation, multiplying with ϕ_i^* on the left, and integrating over all electronic coordinates, we get the following set of coupled equations:

$$[\hat{T}_N + V_i^{\text{ad}} - E] \chi_i = \sum_j \Lambda_{ij} \chi_j. \quad (2)$$

\hat{T}_N is the nuclear kinetic energy operator, V_i^{ad} are the adiabatic electronic energies [$\langle \phi_i^{\text{ad}} | \hat{H}_{el} | \phi_j^{\text{ad}} \rangle = V_i^{\text{ad}}(\mathbf{Q}) \delta_{ij}$] which constitute the PES, and the so-called nonadiabatic coupling operators Λ_{ij} are defined by

$$\Lambda_{ij} = \hat{T}_N \delta_{ij} - \langle \phi_i^{\text{ad}} | \hat{T}_N | \phi_j^{\text{ad}} \rangle. \quad (3)$$

If a specific electronic state ϕ_i^{ad} is energetically well separated from all others, one can neglect the nonadiabatic coupling operators Λ_{ij} .²⁸ This is the famous *Born–Oppenheimer approximation*. The *adiabatic approximation* is defined by additionally neglecting the diagonal term Λ_{ii} . The nonadiabatic coupling operators Λ_{ij} essentially measure the validity of the Born–Oppenheimer approximation, i.e., a sizable Λ_{ij} indicates the intrusion of other electronic states.

In regions of nuclear coordinates where the adiabatic PES approach each other, the Born–Oppenheimer approximation breaks down and the Λ_{ij} cannot be neglected anymore. Generally only a few—in many cases two—electronic states approach each other in a particular region of nuclear coordinate space, i.e., this subset of states is energetically well separated from all other states. Thus, one can employ the *group adiabatic approximation*, that is, neglect only the nonadiabatic coupling operators Λ_{ij} with i being a state from the small subset and j one of the other states. This truncates the sum in Eq. (2) to only those states included in the subset.⁴

We have yet to define the *diabatic* representation (denoted by the superscript “dia”) which allows us to understand the coupling between the states via potentials instead of via momenta as in Eq. (2). To this end we unitarily transform the adiabatic $\{\phi_i^{\text{ad}}\}$ to diabatic states $\{\phi_i^{\text{dia}}\}$ such that $\langle \phi_i^{\text{dia}} | \hat{T}_N | \phi_j^{\text{dia}} \rangle = \hat{T}_N \delta_{ij}$ and thus $\Lambda_{ij} = 0$. We now term the transformed potential energy matrix $\mathbf{V}^{\text{dia}}(\mathbf{Q})$ and get from Eq. (2)

$$[T_N \mathbf{1} + \mathbf{V}^{\text{dia}}(\mathbf{Q}) - E] \chi^{\text{dia}} = 0. \quad (4)$$

Because in general $\mathbf{V}^{\text{dia}}(\mathbf{Q}) = \langle \phi_i^{\text{dia}} | \hat{H}_{el} | \phi_j^{\text{dia}} \rangle$ is not diagonal, the χ_i^{dia} are coupled by the potential energy matrix and are given by the components of the vector χ^{dia} in Eq. (4).

It is clear that the unitary transformation depends on the nuclear coordinates \mathbf{Q} . We may choose a special geometry denoted by \mathbf{Q}_0 —usually the equilibrium geometry of the molecule—for which the adiabatic and the diabatic representations are equivalent (for more details see, e.g., Ref. 4). In the subspace of states obtained by employing the group adiabatic approximation, the transformation will be accomplishable only approximately. But, generally a sufficiently high accuracy can be achieved, in particular in CI situations.^{29–31}

In the following, we will restrict ourselves to a subset of two nondegenerate states; a generalization to more states is straightforward. By extracting a smooth potential $V_0(\mathbf{Q})$,

e.g., in the case of metastable anions one could choose the ground-state potential of the underlying neutral system, we rewrite Eq. (4) in this subset as follows:

$$[\mathbf{H}_0 + \mathbf{V}]\chi^{\text{dia}} = E\chi^{\text{dia}}, \quad (5)$$

where

$$\mathbf{H}_0 = [T_N + V_0(\mathbf{Q})]\mathbf{1}, \quad (6)$$

and

$$\mathbf{V} = \begin{pmatrix} V_1(\mathbf{Q}) & K(\mathbf{Q}) \\ K(\mathbf{Q}) & V_2(\mathbf{Q}) \end{pmatrix}. \quad (7)$$

Herein, $V_{1/2}$ are the diabatic differences in energy between the respective state and V_0 and K is the coupling term between the two states.

B. Coupled PES of metastable electronic states

Metastable states are generally characterized by one of the two following formalisms. The first one was developed and extended by several authors,^{11–14} but is normally referred to as Weisskopf resonance theory. This approach defines resonances as discrete states embedded into and interacting with a continuum. Following this ansatz, a so-called *level shift operator* F_{ij} arises naturally, which additionally to shifting the real part of the energy of the discrete state augments it with an (energy-dependent) imaginary part. A common technique used to compute Weisskopf resonance parameters is Stieltjes imaging.^{8,32,33}

The other possibility is to characterize resonances as so-called Gamow–Siegert eigenstates^{15,16} of the time-independent Schrödinger equation. These grow exponentially in the asymptotic region, describing the decay of the metastable state. As a consequence, the eigenenergies also possess an imaginary part. Siegert energies can be identified with poles of the \mathbf{S} matrix³⁴ and can be calculated, e.g., by the stabilization technique,³⁵ the complex scaling method,³⁶ or the complex absorbing potential approach.^{37–40} The imaginary parts $-i\Gamma/2$ of both the Weisskopf as well as the Siegert energies are related to the lifetime τ of the metastable state by $\tau = \hbar/\Gamma$.

Note that in principle information about resonance states can also be extracted from actual scattering calculations (see, e.g., Ref. 41 for the R -matrix formalism and Ref. 42 for the Schwinger multichannel variational method and the complex Kohn method), but here we consider only methods which give the resonance energy and width directly. The latter methods all exploit the usual Gaussian basis sets and thus in contrast to scattering calculations work entirely in \mathcal{L}^2 space.

Independently of the method used to compute resonances, the calculations provide a set of adiabatic energies which depend on the nuclear coordinates and are complex quantities. Formally, we may proceed as in the preceding subsection and transform the adiabatic resonance states to diabatic ones. There is little, if any, experience in the literature on such transformations for resonance states. Nevertheless, we expect on physical grounds that they do exist. Since the resonance energies are complex, the transformation is not unitary and thus does not lead to a Hermitian (or real sym-

metric) matrix Hamiltonian as obtained in Eq. (7) for bound states—one rather obtains a complex symmetric matrix Hamiltonian.³⁶ We may still use Eqs. (5)–(7), discussed above for bound states, to describe resonances and their dynamics. To this end we just have to assume the elements V_1 , V_2 , and K of the matrix potential \mathbf{V} to be complex quantities.

An alternative derivation of a complex symmetric matrix potential \mathbf{V} is given by Estrada *et al.*¹⁷ Note that they concluded that K has to be real (in particular, they stated that for the off-diagonal elements there is no level shift operator F_{ij}) because of symmetry reasons. But, this is only true in a *strict* two-level system. There are however almost always additional resonance states. Although these states are (in good approximation) vibrationally decoupled from the two states of interest, their presence nevertheless modifies the Hamiltonian of the whole system. In effect, the strict requirement for K to be real is no longer present.

We mention that the set of coupled states used can, in principle, comprise bound and resonance states. Consider, for instance, an anion. This anion can possess bound states as well as resonances, and both types of states can interact via the nuclear motion.⁴³ However, since we are interested here in intersections of PES, the interacting states are all either resonances or bound.

Instead of computing adiabatic resonances and transforming them to diabatic ones, we may also formally start from the assumption that diabatic resonances are given for a manifold of interacting resonances. In this way useful expressions for the diabatic complex potentials $V_{1/2}$, and couplings K can be obtained; see Ref. 17 for details.

A remark is appropriate here. When computing resonances as discrete states embedded into and interacting with a continuum, the resulting quantities $V_{1/2}$ and K depend on the nuclear coordinates and, in addition, also on the total energy of the system. This energy can often be successfully replaced by a function of the nuclear coordinates by going on resonance (for details and references see Ref. 17), eliminating the explicit energy dependence. In some cases, however, it is favorable to use the energy dependence explicitly (see, e.g., Ref. 44). If this is the case, we advocate to follow the formalism described above and the analysis discussed in the following for each value of the total energy separately.

We conclude that Eqs. (5)–(7) could describe as well the coupling between metastable electronic states, provided that these equations contain the respective imaginary terms in $V_{1/2}$ and K .

III. MODEL HAMILTONIANS

A. General properties

An accurate solution of the molecular Schrödinger equation for polyatomic molecules, even in the form given by Eq. (5), generally requires an extreme effort. In practice, one has to make approximations to make the solution feasible. Usually V_0 is approximated to be harmonic in the vicinity of \mathbf{Q}_0 , but the exact form of the ground-state potential is not relevant for our following discussion. Since for each nuclear configuration $V_0(\mathbf{Q})$ is a constant which is added on the

diagonal of the potential matrix \mathbf{V} , it only shifts the eigenenergies of both electronic states by the same amount.

By diagonalizing \mathbf{V} from Eq. (7) we thus obtain the general solution for the adiabatic energy differences between the resonance eigenenergies of the states and the ground state, denoted by V_{\pm}

$$2V_{\pm}(\mathbf{Q}) = \Sigma V(\mathbf{Q}) \pm \sqrt{(\Delta V)^2(\mathbf{Q}) + 4K^2(\mathbf{Q})}, \quad (8)$$

where we introduced the following notation for two arbitrary factors A_1 and A_2 : $\Sigma A = A_1 + A_2$ and $\Delta A = A_1 - A_2$. If we now allow the matrix \mathbf{V} to be complex, Eq. (8) splits into two equations for the real and for the imaginary part of V_{\pm}

$$2 \operatorname{Re}(V_{\pm}(\mathbf{Q})) = \operatorname{Re}(\Sigma V(\mathbf{Q})) \pm \sqrt{\frac{1}{2}(\sqrt{\Re^2(\mathbf{Q}) + \Im^2(\mathbf{Q})} + \Re(\mathbf{Q}))}, \quad (9)$$

$$2 \operatorname{Im}(V_{\pm}(\mathbf{Q})) = \operatorname{Im}(\Sigma V(\mathbf{Q})) \pm \sqrt{\frac{1}{2}(\sqrt{\Re^2(\mathbf{Q}) + \Im^2(\mathbf{Q})} - \Re(\mathbf{Q}))}, \quad (10)$$

with $\Re = \operatorname{Re}((\Delta V)^2 + 4K^2)$ and $\Im = \operatorname{Im}((\Delta V)^2 + 4K^2)$. These quantities were introduced to simplify the calculations and at first sight have no direct physical equivalent, but their significance will become clear below.

Our objective is to find intersections of the complex adiabatic PES $V_{\pm}(\mathbf{Q})$. For this to happen, the square roots in Eqs. (9) and (10) must vanish. It is convenient to start by searching for special points \mathbf{q} in \mathbf{Q} space for which $\Im(\mathbf{q})=0$. For these points, the other relevant quantity $\Re(\mathbf{q})$ appearing in Eqs. (9) and (10) can be either positive, negative, or equal to zero. Accordingly, the following three relationships between $\Re(\mathbf{q})$ and the PES hold:

$$\Re(\mathbf{q}) \begin{cases} < 0 \\ > 0 \\ = 0 \end{cases} \Leftrightarrow \begin{cases} \operatorname{Re}(V_+(\mathbf{q})) = \operatorname{Re}(V_-(\mathbf{q})) \\ \operatorname{Im}(V_+(\mathbf{q})) = \operatorname{Im}(V_-(\mathbf{q})) \\ V_+(\mathbf{q}) = V_-(\mathbf{q}). \end{cases} \quad (11)$$

If $\Re(\mathbf{q})$ is positive, the imaginary parts of the PES intersect, but the real parts do not. The opposite holds if $\Re(\mathbf{q})$ is negative. Only for both $\Re(\mathbf{q})=0$ and $\Im(\mathbf{q})=0$ both the imaginary and real parts of the PES intersect.

Let us discuss this finding first before we introduce some model Hamiltonians by giving explicit expressions for $V_{1/2}$ and K . Assumed that there is an interval of points $\{\mathbf{q}\}$ for which $\Im(\mathbf{q})=0$ holds, there generally will be more than one point for which $\Re(\mathbf{q})<0$ is satisfied. In the case of PES of bound states, conical intersections are of dimension $\mathcal{N}-2$, with \mathcal{N} being the number of nuclear degrees of freedom.⁴ Apparently this no longer holds for the real part of the eigenenergy $\operatorname{Re}(V_{\pm})$! Already in the two-dimensional case there generally is a seam of intersections in the real part of V_{\pm} . Following the same line of argument, it follows that there is in general also a seam of intersections for the imaginary part of the eigenenergy.

These seams meet at special generalized points (if they exist) for which $\Re(\mathbf{q})$ is zero, too. Here, “generalized point” is meant to be an object of dimension $\mathcal{N}-2$. Since they represent the complex analog of conical intersections, we will call all the “points” \mathbf{q} , for which $\Im(\mathbf{q})=\Re(\mathbf{q})=0$ holds, the *complex conical intersection* (CCI) points in the following.

Note that there could be special cases of \mathbf{V} for which there are no or only a finite number of points \mathbf{q} for which $\Im(\mathbf{q})=0$ and $\Re(\mathbf{q})$ less than, greater than, or equal to zero holds. But, as we will see below, $\Im(\mathbf{q})=0$ is easily satisfied and in general there will be an infinite number of points for which $\Re(\mathbf{q})$ is less or greater than zero and more than one point for which $\Re(\mathbf{q})=0$ holds if one makes reasonable assumptions for the expressions for V_i and K . For example, Estrada *et al.* already observed the real and imaginary seams mentioned above with their simple two-dimensional model Hamiltonian for two interacting resonance states (see Sec. III C and Ref. 17).

We now continue with some model Hamiltonians which will clarify the points discussed above. The first step is to restrict ourselves to two nuclear modes denoted by Q_g and Q_u , which can be chosen to be normal coordinates of the molecule in its ground state. The labeling Q_g is chosen to denote a totally symmetric vibrational mode which is responsible for the energy difference $V_2 - V_1$. Because of this it is also called the “tuning” mode, whereas Q_u is termed the “coupling” mode.⁴ The latter is chosen to be a nontotally symmetric vibrational mode, with the only restriction that the direct product of the irreducible representations of the two states and of Q_u contains the totally symmetric representation Γ_A

$$\Gamma_A \in \Gamma_1 \times \Gamma_u \times \Gamma_2. \quad (12)$$

Let us further assume that $V_{1/2}$ and K in Eq. (7) are slowly varying functions of Q_g and Q_u in the vicinity of \mathbf{Q}_0 . This makes an expansion of $V_{1/2}$ and K in these two coordinates possible. Note that these expansions are restricted for symmetry reasons. The fact that the potential term \mathbf{V} of Eq. (7) has to be totally symmetric leads to the restriction that $V_{1/2}$ have to be even in Q_u and that K has to be odd in Q_u . Strictly, this holds true only for Abelian point groups, but for degenerate groups a similar argument can be employed.

B. Usual conical intersection

In order to make the differences between intersecting PES of bound and resonance states more clear, we briefly review the former case first. For bound states, the terms $V_{1/2}$ and K up to linear order are given by⁴

$$V_i = E_i + \kappa_i Q_g, \quad i = 1, 2; \quad (13)$$

$$K = \lambda Q_u.$$

Since there is no imaginary part, only the condition $(\Delta V)^2 = -4K^2$ has to be fulfilled for intersections to occur between the adiabatic PES. We easily see that this is the case for only *one* point $(Q_g^{\text{CI}}, Q_u^{\text{CI}})$ (apart from accidental degeneracies), where

$$Q_g^{\text{CI}} = -\frac{\Delta E}{\Delta \kappa} \quad \text{and} \quad Q_u^{\text{CI}} = 0, \quad (14)$$

using the notation introduced above, i.e., $\Delta E = E_1 - E_2$ and $\Delta \kappa = \kappa_1 - \kappa_2$.

C. Minimal model for resonances

The simplest complex model Hamiltonian which makes sense physically is obtained by setting

$$V_i = E_i + \kappa_i Q_g - \frac{i}{2} \Gamma_i, \quad i=1,2; \quad (15)$$

$$K = \lambda Q_u.$$

This is equivalent to the model example discussed by Estrada *et al.*¹⁷ and we will call this choice the “minimal model” in the following. Compared to Sec. III B, only the terms $-i\Gamma_i/2$ were added, corresponding to widths which are independent of the positions of the nuclei. The implications of this slight modification were discussed extensively in Ref. 17 and we will only summarize the points relevant to our discussion here.

The most startling result is that there is no longer *one* conical intersection point $(Q_g^{\text{CI}}, Q_u^{\text{CI}}) = (-\Delta E/\Delta\kappa, 0)$ as in case of bound states (see Sec. III B), but *two* points $(Q_g^{\text{CCI}}, \pm Q_u^{\text{CCI}})$ for which $V_+ = V_-$ holds true. These points lie symmetrically to the Q_g axis and are given by

$$Q_g^{\text{CCI}} = -\frac{\Delta E}{\Delta\kappa} \quad \text{and} \quad Q_u^{\text{CCI}} = \frac{\Delta\Gamma}{4\lambda}, \quad (16)$$

i.e., $Q_g^{\text{CCI}} = Q_g^{\text{CI}}$ still holds in the minimal model.

The two CCI points are connected by a straight line formed by the seam of intersections of the real part of V_{\pm} which was already mentioned in Sec. III A. The seam of intersections of the imaginary part of V_{\pm} which was also discussed above has two branches which start from the two intersecting points, and go to $\pm\infty$ from there on in a straight line.

We picture the real and the imaginary parts of V_{\pm} in Fig. 1. It is important to note the difference from Fig. 2 in Ref. 17, stemming from a slightly different notation: There, the PES *including* the ground-state potential were shown, whereas in our Fig. 1 only the differences $V_{\pm} = V_i^{\text{ad}} - V_0$ are pictured. We do this to simplify the comparison with the PES of the following, more complicated model Hamiltonians. Also shown in Fig. 1 is a projection of the real (solid line) and the imaginary (dashed line) seams of intersections onto the $Q_g Q_u$ plane. This projection will also simplify the comparison in between the different model Hamiltonians. In this picture we marked the CCI points with crosses and the point $-\Delta E/\Delta\kappa$ on the Q_g axis with a filled circle.

The two parts of the PES are shown only for positive values of Q_u , since the other halves are simply obtained by taking the mirror image at the plane consisting of the Q_g axis and the respective z axis. This also allows us to make another important result more clearly visible: The imaginary PES are discontinuous over the whole range of points which form the real seam. This interesting result was not discussed in Ref. 17 and we will see below that the discontinuity apparently is no artifact of the oversimplified nature of the model Hamiltonian.

D. Linear widths

The most obvious modification of the minimal model is to include a dependency of the widths on the positions of the nuclei. In lowest order one thus obtains

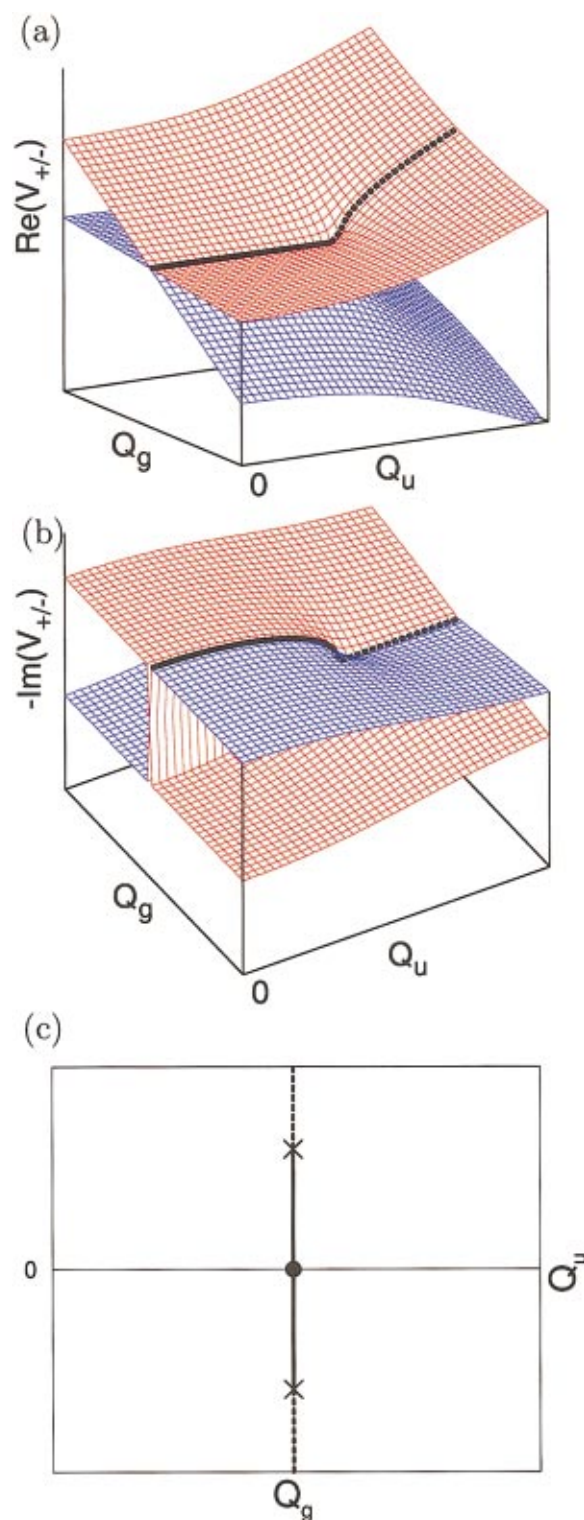


FIG. 1. (Color) PES for the minimal model. (a) shows the real parts and (b) the imaginary parts of the complex adiabatic PES given by $V_{\pm}(Q_g, Q_u)$. The position of the real seam is marked with a solid line in *both* pictures to guide the eye. The same holds for the imaginary seam for which a dashed line was chosen. Note that the PES are only shown for positive values of Q_u in (a) and (b) to uncover the discontinuity in the imaginary parts (see the text). A projection of the seams onto the $Q_g Q_u$ plane yields figure (c). It also shows the half plane for which $Q_u < 0$ and thus demonstrates the symmetry of the PES to the Q_g axis. In (c), we marked the CCI points with crosses and the coordinates for which the real seam crosses the Q_g axis with a filled circle.

$$V_i = E_i + \kappa_i Q_g - \frac{i}{2}(\Gamma_i + \alpha_i Q_g), \quad i=1,2; \quad (17)$$

K as in Eq. (15). Note that we have to set $\Gamma_i + \alpha_i Q_g = 0$ for values of Q_g for which this term becomes less than zero, since negative widths make no sense physically.

The adiabatic PES which are the solutions for this choice of \mathbf{V} and the projection of the seams are shown in Fig. 2. As is clearly seen, there are now *two* solutions for $\Im(Q_g, Q_u) = 0$, namely

$${}^{(1)}Q_g = -\frac{\Delta E}{\Delta \kappa} \quad \text{and} \quad {}^{(2)}Q_g = -\frac{\Delta \Gamma}{\Delta \alpha}, \quad (18)$$

with ${}^{(1)}Q_g$ being the same solution as Q_g^{CCI} in the minimal model. Whether ${}^{(1)}Q_g < {}^{(2)}Q_g$ (as in Fig. 2) or the opposite applies can only be decided if explicit parameters are given. In the projection picture we additionally marked the second solution ${}^{(2)}Q_g$ with an empty circle.

The real parts of the PES in Fig. 2 are at first sight the same as for the minimal model, but there is a slight difference: The CCI points are now found at $(Q_g^{\text{CCI}}, \pm Q_u^{\text{CCI}})$ with

$$Q_g^{\text{CCI}} = {}^{(1)}Q_g \quad \text{and} \quad Q_u^{\text{CCI}} = -\frac{\Delta E}{\Delta \kappa} \frac{\Delta \alpha}{4\lambda} + \frac{\Delta \Gamma}{4\lambda}. \quad (19)$$

Additionally, there is a second seam of intersections. It is found to be a straight line at $Q_g = {}^{(2)}Q_g$ completely lying in the imaginary parts of the PES. Also note that $\Re(Q_g, Q_u)$ depends on Q_u quadratically, contrary to $\Im(Q_g, Q_u)$ which is independent of Q_u . Looking at Eq. (10) it follows that $\text{Im}(V_+) - \text{Im}(V_-) \rightarrow 0$ for $Q_u \rightarrow \infty$, independently of the value of Q_g . This is the same behavior already observed in the minimal model (see Fig. 1 and Ref. 17). Additionally, we also find a discontinuity in the imaginary parts of the PES similar to the discontinuity in the minimal model.

E. Complex coupling

As discussed at the end of Sec. III A, the coupling term could as well be complex. We thus chose the following expression:

$$K = \lambda Q_u - \frac{i}{2} \eta Q_u, \quad (20)$$

$V_{1/2}$ as in Eq. (15). In Fig. 3, we again show the real and imaginary parts of the PES together with the projection picture.

At first glance the only difference to the minimal model is that the seams no longer lie on a straight line but on a “outwardly” bent *parabola*. The curvature depends on the sign of the term $\eta(\Delta\Gamma/4\lambda)$. For $\eta(\Delta\Gamma/4\lambda) > 0$ one arrives at the situation pictured in Fig. 3; if the term is less than zero, the parabola is bent “inwards.” This holds if one restricts oneself (without losing generality) to the case $E_1 > E_2$ and

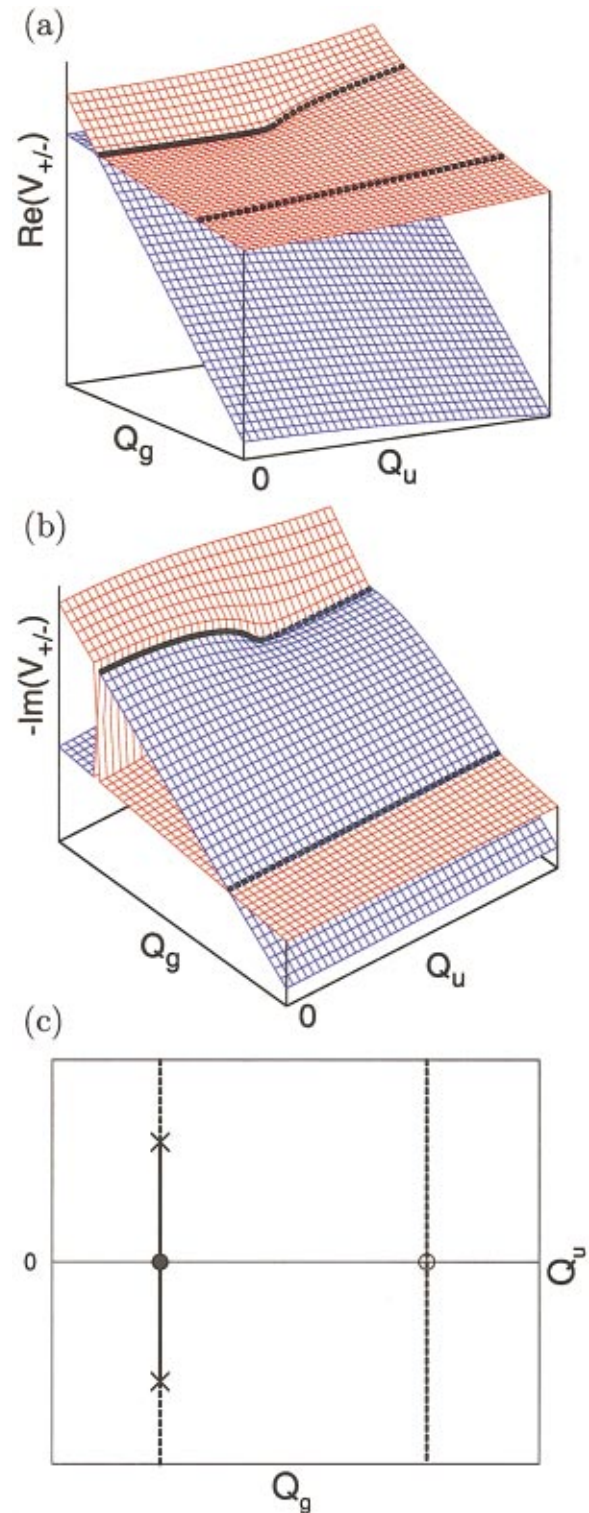


FIG. 2. (Color) PES for the linear widths model. (a)–(c) are pictured the same way as in Figs. 1, 3, and 5 and allow a direct comparison of the models. Most interesting is the appearance of a second imaginary seam. The position at which this seam crosses the Q_g axis is marked with an empty circle in (c). Also note that $\text{Im}(V_+) - \text{Im}(V_-) \rightarrow 0$ for $Q_u \rightarrow \infty$ still holds as in the minimal model.

$\Delta\kappa < 0$, effectively placing the intersection of the real parts for $Q_u = 0$ [the black dot in Fig. 3(c)] at a positive value for Q_g , namely at $Q_g = -\Delta E / \Delta\kappa > 0$. We conclude that the complex-coupling model is equivalent to the minimal model (and to the linear widths model) there. This immediately be-

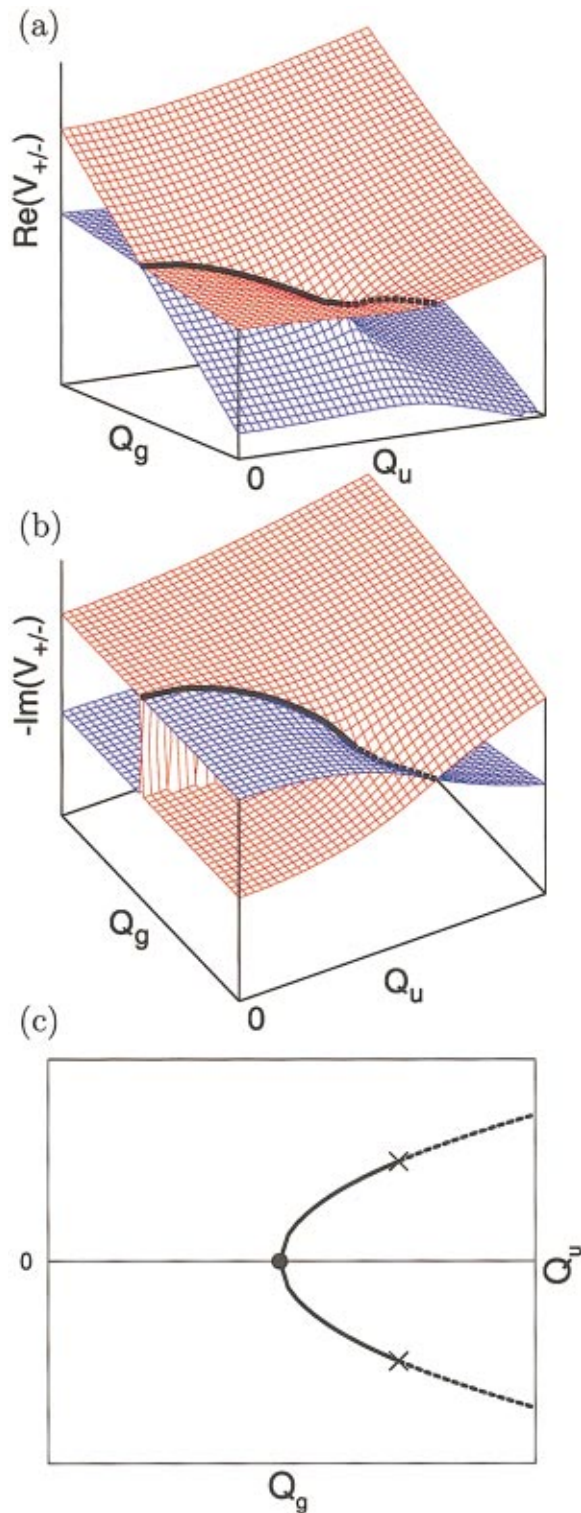


FIG. 3. (Color) PES for the complex coupling model. (a)–(c) are pictured the same way as in Figs. 1, 2, and 5 and allow a direct comparison of the models. The most obvious new feature is a bending of the line which is formed by the seams. Another difference is that now $\text{Im}(V_+) - \text{Im}(V_-) \rightarrow \infty$ for $Q_u \rightarrow \infty$. This behavior is only found for the *real* parts of the PES in the minimal and the linear widths models.

comes clear by looking at the expressions for K which are zero at $Q_u = 0$.

The CCI points are placed at $(Q_g^{\text{CCI}}, \pm Q_u^{\text{CCI}})$, which are now given by

$$Q_g^{\text{CCI}} = -\frac{\Delta E + \eta \frac{\Delta \Gamma}{4\lambda}}{\Delta \kappa} \quad \text{and} \quad Q_u^{\text{CCI}} = \frac{\Delta \Gamma}{4\lambda}, \quad (21)$$

i.e., the solution for Q_u^{CCI} stays the same as in the minimal model. As can be easily checked, $\sqrt{\Re^2 + \Im^2} - \Re \rightarrow (2\lambda - \eta)^2 Q_u^2$, i.e., $\text{Im}(V_+) - \text{Im}(V_-) \rightarrow \infty$ for $Q_u \rightarrow \infty$ (excluding the points on the imaginary seam). Such a behavior is found only for the *real* part of the energy in the minimal and the linear widths models, whereas $\text{Im}(V_+) - \text{Im}(V_-) \rightarrow 0$ for $Q_u \rightarrow \infty$ holds in those two models. We again observe that there is a discontinuity in the imaginary parts of the PES.

F. Complete linear model

Let us see what happens if one combines a linear ansatz for the widths with a complex linear coupling term. To recollect, we now have

$$V_i = E_i + \kappa_i Q_g - \frac{i}{2} (\Gamma_i + \alpha_i Q_g), \quad i = 1, 2; \quad (22)$$

$$K = \lambda Q_u - \frac{i}{2} \eta Q_u.$$

Before we start to evaluate this model in detail, let us first give some additional definitions and a small constraint, which does not restrict generality but makes the discussion simpler. We easily see that the intersections for $Q_u = 0$ are at $Q_g = -\Delta E / \Delta \kappa$ for the real parts of the PES, and at $Q_g = -\Delta \Gamma / \Delta \alpha$ for the imaginary parts. These are the same coordinates as in Sec. III D and here we introduce the abbreviations $Q_g^{\text{Re},0} = -\Delta E / \Delta \kappa$ and $Q_g^{\text{Im},0} = -\Delta \Gamma / \Delta \alpha$. If we require both $Q_g^{\text{Re},0}$ and $Q_g^{\text{Im},0}$ to be positive and suppose $E_1 > E_2$, it follows that $\Delta \kappa < 0$ and $\Delta \Gamma \Delta \alpha < 0$. The factor on which the shape of the PES depends is again (as in Sec. III E) the sign of $\eta(\Delta \Gamma / 4\lambda)$. But, here one can as well employ the sign of $\eta(\Delta \alpha / 4\lambda)$ for the characterization of the PES, which is just the opposite. Additionally, the magnitude of $\Delta \kappa$ in relation to the magnitude of $\eta(\Delta \alpha / 4\lambda)$ becomes important as we will see below.

Employing the restriction given above, one can still distinguish eight different cases, which can be further grouped into two sets of four cases each. For the first set, we only show the projection of the seams onto the $Q_g Q_u$ plane for one example in Fig. 4. The projection of the seams now forms the two branches of a *hyperbola*. The parameters are chosen in such a way that $Q_g^{\text{Re},0} < Q_g^{\text{Im},0}$ and $0 < \eta(\Delta \alpha / 4\lambda) < |\Delta \kappa|$. The other three cases of this set can be obtained by changing the ordering of the terms in these two inequalities, but always keeping $\eta(\Delta \alpha / 4\lambda)$ greater than zero. Graphically this corresponds to either interchanging the dashed and solid lines (i.e., the real and imaginary seams), or to taking the mirror image of the seams at a line parallel to the Q_u axis through the middle of $Q_g^{\text{Re},0}$ and $Q_g^{\text{Im},0}$, or to both of these operations.

All four cases of this set are similar to the two models discussed before in the sense that there are again *two* distinct seams as in Sec. III D, one of which is either located totally in the imaginary parts of the PES or totally in the real parts.

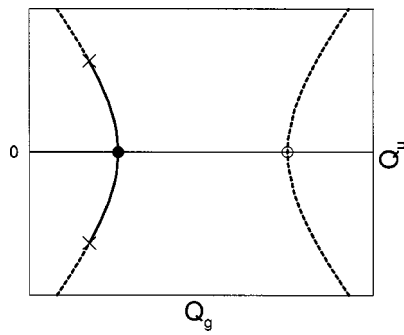


FIG. 4. Example of PES for the complete linear model with $\eta(\Delta\alpha/4\lambda) > 0$ (see the text). We only show the corresponding projection picture (see Figs. 1–3, 5) since the PES are similar to the linear widths and the complex coupling model, respectively. This is demonstrated by the fact that there is an additional imaginary seam, like in the linear widths model (see Fig. 2), which is bent, as in the complex coupling model (see Fig. 3).

Both seams are also *bent* as the single seam in Sec. III E. But, since they are always bent away from each other, the seams again extend to $Q_u = \pm\infty$.

The question arises if it is possible to restrict the interaction domain to a finite region within the linear order approximation. This can indeed be achieved for the four cases of the second set. One of these cases is pictured in Fig. 5; there we again show the real parts of the PES, the imaginary parts, and the projection of the seams. As can be seen, this set features an all new shape of the PES: the seams now form a closed loop. This loop is an *ellipse*, as can be seen from the equation

$$Q_u^2 = -(4\eta\lambda)^{-1}(\Delta E + \Delta\kappa Q_g)(\Delta\Gamma + \Delta\alpha Q_g), \quad (23)$$

which is obtained by setting $\Im(Q_g, Q_u) = 0$.

For the case which is pictured in Fig. 5, the parameters are chosen in such a way that $Q_g^{\text{Re},0} < Q_g^{\text{Im},0}$ and $\Delta\kappa < \eta(\Delta\alpha/4\lambda) < 0$. The other three cases are again obtained by exchanging the solid and dashed lines, i.e., the real and imaginary seams in the projection picture, or by taking the mirror image of the seams as described above, or by employing both of these operations. This again corresponds to changing the ordering of the terms in the inequalities, but now always keeping $\eta(\Delta\alpha/4\lambda) < 0$.

In all of the eight cases there are still exactly two points $(Q_g^{\text{CCI}}, \pm Q_u^{\text{CCI}})$, given by

$$Q_g^{\text{CCI}} = -\frac{\Delta E + \eta \frac{\Delta\Gamma}{4\lambda}}{\Delta\kappa + \eta \frac{\Delta\alpha}{4\lambda}} \quad \text{and} \quad Q_u^{\text{CCI}} = \frac{-\Delta E \Delta\alpha + \Delta\Gamma \Delta\kappa}{4\lambda \Delta\kappa + \eta \Delta\alpha}, \quad (24)$$

which connect the real and imaginary seams. The discontinuity of the imaginary parts at the coordinates of the real seam is also still present in all eight cases, see, e.g., Fig. 5.

G. Discussion

As we have seen in the preceding subsections, small extensions of the minimal model Hamiltonian in Eq. (15) lead to profound changes in the PES. In particular, changing the widths from constants to linear functions of Q_g caused an

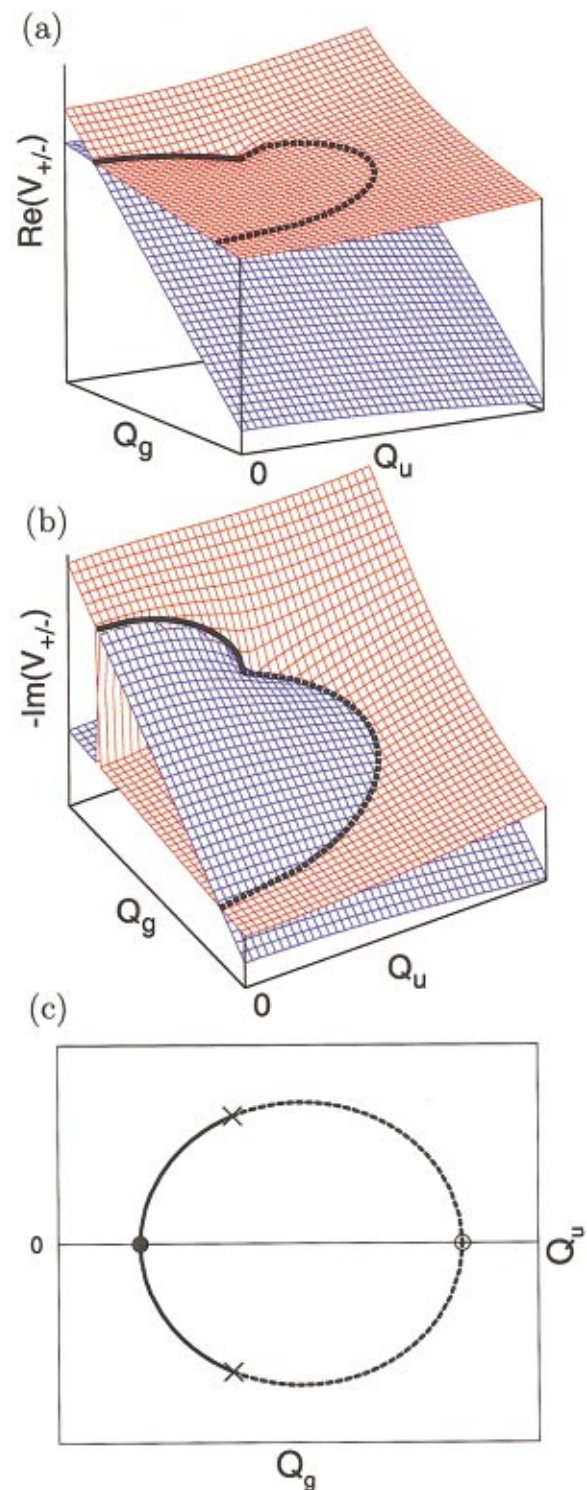


FIG. 5. (Color) Example of PES for the complete linear model with $\eta(\Delta\alpha/4\lambda) < 0$ (see the text). (a)–(c) are pictured the same way as in Figs. 1–3 and allow a direct comparison of the models. Note that the real and imaginary seam now form a closed loop, i.e., the interaction region is finite. However, the discontinuity in the imaginary parts is still present.

extra imaginary seam to appear, whereas the introduction of a complex coupling linear in Q_u led to the bending of the original seams. All three of these models show imaginary seams extending to $Q_u = \pm\infty$. But, this poses no problem, since we only investigate expansions of \mathbf{V} [Eq. (7)] in the

vicinity of \mathbf{Q}_0 here. In reality, $K \rightarrow 0$ for $Q_u \rightarrow \infty$ holds, i.e., for large values of Q_u the PES indeed intersect no more.

By combining the two extensions mentioned above and constraining the parameters to certain values, we arrived at PES for which the real and imaginary seams form a closed loop. Let us mention that our study of another model Hamiltonian not presented here demonstrated that a bending of the seams can also be enforced, e.g., by adding quadratic terms in Q_u to $V_{1/2}$, but the introduction of a complex coupling seems to be the conceptually easiest and most natural way to arrive at a closed loop of the seams. Note a mathematical curiosity: for PES of bound states, the intersection has the form of a double cone, whereas for PES of metastable states the models with a complex coupling yield intersection seams with the shape of a parabola, hyperbola, or an ellipse. These three forms actually can be obtained by cutting a double cone with a plane.

We are still faced with the discontinuity of the imaginary parts of the PES (see Fig. 5). To investigate this phenomenon further, we also tried more complicated models which incorporate higher order terms of Q_g and Q_u in $V_{1/2}$ and K . These model Hamiltonians have the drawback that they are in general not analytically solvable anymore. Apart from this, the discontinuity does not disappear with these more sophisticated models. We are thus left with the view that it seems to be an intrinsic feature of the adiabatic picture. In order to check if this discontinuity can be reproduced by *ab initio* data, we chose to investigate a practical example. The complex PES obtained for this example and their relation to the model Hamiltonian will be described in detail in the next section.

Finally, note that all models investigated have in common that always *exactly two* CCI points exist, connecting the real and imaginary seams. This appears to be a general phenomenon and maybe is as common as the real analog, namely two PES forming a conical intersection. We thus term this special behavior of two complex PES, in particular the most general model presented in Sec. III F, *doubly intersecting complex energy surfaces* (DICES). It is important to note that the nonadiabatic coupling operators Λ_{ij} are singular at these two CCI points—the same behavior also found at a conical intersection in between PES of bound states.⁴ This was already shown by Estrada *et al.* for the minimal model Hamiltonian¹⁷ and still holds for the more advanced model Hamiltonians presented here. Thus, the adiabatic approximation breaks down at the CCI points and one indeed has to employ the group adiabatic approximation.

IV. PRACTICAL EXAMPLE: CHLOROETHENE ANION

The chloroethene anion turned out to be an excellent example to investigate the occurrence of DICES in a real molecule. This is because several experimental observations led to the proposal that it possesses a Σ^* -type (${}^2A'$) as well as a Π^* -type (${}^2A''$) resonance state which cross near the equilibrium geometry of the corresponding neutral (see, e.g., Refs. 45, 46).

In electron transmission studies, dissociative electron attachment (DEA) was observed, leading to a ethenyl radical

and a chloride anion. Similar processes have been found to occur in many other unsaturated organic compounds which have in common that a halogen atom is connected to one of the carbon atoms involved in the double bond. Examples are chlorobenzene,^{24,47,48} mono- to tetrachloroethene,^{48–50} and chlorouracil.^{25,26} DEA to the latter is discussed as an important contribution to radiation damage to DNA.^{25,51} Furthermore (unsaturated) halogenated hydrocarbons have become a major threat to the environment and the DEA process appears to be an economic way of eliminating the halogen atom (see, e.g., Christophorou and Hunter in Ref. 52, p. 318). Note that DEA is not limited to unsaturated organic molecules containing halogen atoms (for recent reviews including many other examples, see, e.g., Refs. 53–55).

The DEA process is thought to occur in the following way. First, the electron is captured into the π^* orbital of the unsaturated carbon–carbon bond. This results in a resonance state which is energetically lower lying and possesses a longer lifetime than the metastable state obtained from the capture into the σ^* orbital of the carbon–halogen bond. The electron is then transferred into the σ^* orbital at a nuclear configuration where the lifetime of the corresponding repulsive state is long enough to eventually lead to the dissociation of the molecule. This transfer process is said to occur via nuclear motion. Only a few publications have dealt with the details of the process up to now (see, e.g., Refs. 46, 56, 57). In particular, no theoretical work at all has been published which explicitly takes into account the metastable nature of the system. But, the essential part of a theoretical description of the DEA process is concerned with this metastability and requires the computation of the complex PES.

In the following we will briefly explain our computational method for obtaining the *ab initio* data for the PES of the resonance states of the chloroethene anion. After outlining our method, we try to fit the PES obtained from the model Hamiltonian in Sec. III F to our *ab initio* data, both for testing our model and for providing an analytical expression for the complex PES required for a molecular dynamics description of the DEA process. Note that the chloroethene anion is the prototype for all halogenated, unsaturated organic molecules, because it consists of only two doubly bound carbon atoms to which a chlorine atom is connected. The three hydrogen atoms which saturate the remaining bonds lie in the same plane, resulting in a C_s symmetric structure.

A. Computational methods

We first optimized the geometry of the neutral chloroethene at the Hartree–Fock (HF) self-consistent field (SCF) level of theory employing the standard 6-31G* basis set. This geometry was taken to be the equilibrium geometry \mathbf{Q}_0 (see Sec. II) in the following calculations. The standard calculations were done within the framework of the GAMESS UK 6.2.1⁵⁸ and MOLCAS 5⁵⁹ *ab initio* packages of programs.

The complex energy surfaces were calculated using our newly developed method CAP/ $\Sigma^{(2)}$. This efficient technique to calculate resonance energies and widths for temporary anions was described in detail in Ref. 40 and we will only give a short overview of this method here. In the following we

will use some terms, e.g., η and Σ , which are not to be confused with the quantities introduced in Sec. III.

As mentioned in Sec. II, Gamow–Siegert states grow exponentially in the asymptotic region. This makes their description by \mathcal{L}^2 basis sets, like the Gaussian basis sets implemented in all standard quantum chemistry programs, impossible. One possibility to overcome this problem is to add a complex potential $-i\eta W$ with a strength parameter η to the Hamiltonian H_0 of the system, which “absorbs” the outgoing wave at a distance from the molecule. Because of this it is termed *complex absorbing potential* (CAP).

One can define a one-particle Green’s function⁶⁰ corresponding to this modified Hamiltonian. As shown explicitly in Ref. 61, this Green’s function can be evaluated using perturbation theory, in particular employing the algebraic diagrammatic construction scheme up to 2nd (or 3rd) order (ADC(2/3)^{62,63}). By a projection of the resulting CAP/ADC(2)-matrix on the one-particle space, a simple, complex symmetric Hamiltonian of small dimension was obtained:⁴⁰

$$H = H_0 + \Sigma^{(2)}(E) - i\eta W. \quad (25)$$

Here, $\Sigma^{(2)}(E)$ is the so-called self-energy⁶⁰ in second order, which is energy dependent. Together with the CAP term it represents an optical potential (see, e.g., Refs. 8, 64 and references therein) for electrons which are bound temporarily to the system.⁴⁰ This explains the designation CAP/ $\Sigma^{(2)}$.

The exact procedure to obtain the energies and widths of the resonance states was described in detail in Ref. 40. In short, the eigenvalues of the energy-dependent, complex-symmetric eigenvalue problem defined by the Hamiltonian in Eq. (25) are calculated for varying values of η and a resonance state can be identified with a stabilization point in the η trajectories. The real part of its respective eigenvalue is equivalent to the negative of a electron attachment energy, whereas its imaginary part gives the lifetimes of the corresponding metastable anion. We found that the CAP/ $\Sigma^{(2)}$ method reproduces experimental electron attachment energies measured by electron transmission spectroscopy⁶⁵ within a few tenths of an eV. The error introduced by using finite basis sets was estimated to be of the order $\pm 5\%$ for the energies and $\pm 25\%$ for the widths.⁴⁰

The method is suited to investigate the crossing of the complex PES of the chloroethene anion in detail. We employed a box-CAP,⁶⁶ which started to increase 3 a.u. “outside” the molecule in each Cartesian direction, and the double-zeta basis set by Dunning and Hay⁶⁷ for our calculations. This basis set was further augmented with two d -type (exponents 1.097 and 0.318 for C, 1.046 and 0.344 for Cl) and one f -type (exponent 0.761 for C and 0.706 for Cl) polarization functions, and one s -type diffuse function (exponent 0.0765 for C and 0.0942 for Cl) on each heavy atom. To describe the continuum part of the resonances properly, eight even-tempered (factor 1.6) diffuse p -type functions were also added on each carbon and on the chlorine atom, starting from the exponents 0.1146 and 0.1838, respectively. After discarding the core and anticore orbitals we finally arrived at 111 molecular orbitals of A' symmetry and 47 of A'' symmetry, which coalesce into 158 orbitals when the symmetry of the

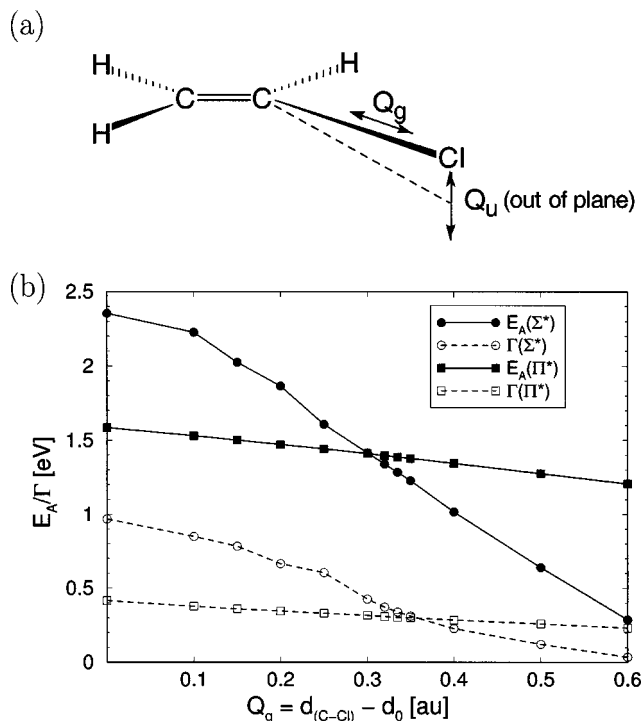


FIG. 6. *Ab initio* data on the chloroethene anion. (a) Definition of Q_g and Q_u . Both are measured relative to the equilibrium geometry of neutral chloroethene. (b) Dependency on Q_g ($Q_u=0$) of the negative electron attachment energies (solid lines) and the widths (dashed lines) of the Σ^* (circles) and Π^* (squares) resonances of the chloroethene anion. The lines are only drawn to guide the eye. Note the wiggles in the curves for the Σ^* resonance which originate from the effective change of basis during the elongation of the C–Cl bond.

molecule is lowered by deflection of the chlorine atom out of the molecular plane.

B. Results

We calculated the Siegert energies at 110 different nuclear configurations, i.e., for 110 points (Q_g, Q_u) . As shown in Fig. 6(a), Q_g corresponds to the elongation of the C–Cl bond, whereas Q_u is the angle in between the C–Cl bond and the plane defined by the remaining atoms. Q_g lies in between 0.0 and 0.8 a.u. and Q_u ranges from 0.0° to 10.0°. We solved the electronic problem at each distinct nuclear configuration and thus obtained the adiabatic PES. The obtained data showed clear signs of only two resonance states lying energetically close to another, which allowed us to make use of the complete linear model Hamiltonian introduced above.

In Fig. 6(b), we show the dependence of the negative electron attachment energies and the widths of the Σ^* and the Π^* resonance states on Q_g , i.e., a cut through the PES at $Q_u=0$. The attachment energies are drawn as solid lines and with filled symbols, whereas the dashed lines with empty symbols represent the widths. Energies and widths corresponding to the Σ^* resonance are symbolized by circles, whereas squares were chosen for the respective graphs for the Π^* resonance. At the equilibrium geometry of the neutral chloroethene ($Q_g=0$) we find an electron attachment energy of 2.36 eV for the Σ^* state, compared to values of 2.84

TABLE I. Parameters obtained from the fit of *ab initio* data for the resonance states of the chloroethene anion to the complete linear model (see the text). In total 76 points (Q_g, Q_u) were used, i.e., 152 energies and 152 widths. E_i and Γ_i are in eV, κ_i and α_i in eV/a.u., and λ and η in eV/radian.

i	1	2
E_i	2.563	1.608
Γ_i	1.254	0.404
κ_i	-3.827	-0.661
α_i	-2.728	-0.303
λ		1.717
η		1.112

eV^{48,49} and 2.9 eV⁴⁶ given by experimentalists. The respective values for the Π^* state are 1.59 eV from our calculation and 1.2 eV,⁵⁰ and 1.28 eV^{46,48,49} from experimental data. Of course, due to the vibronic excitations present in the experiment, vertical electron attachment energies cannot be deduced from the experiments directly, and the experimental values can only be considered as estimates. Another possible origin for the deviation between the calculated and experimental data is discussed below, with special regard to the different sign of the deviation for the Σ^* and Π^* states. For metastable states of molecules of this size the results are however of acceptable accuracy.

Note the small “wiggles” in the curves of the energy and the width of the Σ^* resonance state. This results from the fact that we found *two* stabilization points in the η trajectories (see Sec. IV A) for nearly every point (Q_g, Q_u) and in the majority of cases could not decide which one was the right one. Since together the two points formed a relatively broad double minimum in the “velocity” of the η trajectory instead of the usual single distinct minimum, both stabilization points yielded energies and widths which were very similar. But, even choosing in each case the one which gave the most smooth curves still resulted in the wiggles shown in Fig. 6. This problem can be explained by the realization that by elongation of the C–Cl bond, the basis functions placed on the Cl atom are moved together with the atom, effectively resulting in a change of the basis set. The use of a larger basis set presumably would solve this problem but is not practical for the calculation of the large number of points required for our purpose.

Luckily, the wiggles are not pronounced in the interaction region of the two resonance states. We thus restrict ourselves to values of Q_g in between 0.25 and 0.4 a.u. and further to values of Q_u less than 2° , satisfying the requirement of small deflections. The resulting 76 points, corresponding to in total 152 electron attachment energies and 152 widths, were used for a fit to the complete linear model discussed in Sec. III F to quantify the ten parameters E_i , κ_i , Γ_i , α_i ($i = 1, 2$) and λ , η . The results are summarized in Table I.

With a value of 0.024 for the sum of squared differences, corresponding to a standard deviation of 9 meV, the fit is relatively good. Using the obtained parameters, we find the following explicit values: $Q_g^{\text{Re},0} = 0.3016$ a.u., $Q_g^{\text{Im},0} = 0.3503$ a.u., $Q_u^{\text{CCI}} = 0.3070$ a.u., and $Q_u = 0.8766^\circ$.

In Fig. 7 we compare the PES from the fit with the *ab initio* data for some cuts through the PES orthogonal to the

Q_g axis, i.e., along Q_u . Figure 7(a) is a blowup of the relevant region of Fig. 6. There are, however, some important differences: circles now represent the upper (i.e., energetically higher) PES and squares the lower PES as the assignment to Σ^* or Π^* no longer makes sense for $Q_u \neq 0$. The points are *ab initio* data, whereas the curves are PES drawn according to the fit to the model Hamiltonian. We also marked the positions of the cuts orthogonal to the Q_g axis in Fig. 7(a).

Figure 7(b) shows the first of these cuts and is located at $Q_g = 0.3$ a.u., i.e., very close to $Q_g^{\text{Re},0}$. We see that the real PES nearly cross and that the imaginary PES approach each other at about $Q_u = 1^\circ$. This value of Q_u is very similar to Q_u^{CCI} (see above). Cut (c) at $Q_g = 0.304$ a.u. is situated in between $Q_g^{\text{Re},0}$ and Q_g^{CCI} , and shows two points of the real seam at approximately $Q_u = \pm 0.75^\circ$ and the discontinuity in the imaginary seam at the same location in Q_u . The third cut displayed in Fig. 7(d) lies shortly behind Q_g^{CCI} at $Q_g = 0.308$, i.e., the real parts of the PES have just separated. The imaginary parts no longer show a discontinuity, but two simple crossing points (out of the imaginary seam), which of course lie symmetrically to the Q_g axis. In cut (e) at $Q_g = 0.335$ the distance in direction of Q_u in between the two imaginary crossing points is almost at its maximum, whereas the two real PES are now smooth curves which no longer show any direct sign of interaction. At $Q_g = 0.35$, the absence of interaction in between the real PES is perhaps even more apparent as Fig. 7(f) shows almost straight lines. The imaginary PES are shortly before separating because $Q_g^{\text{Im},0}$ is only slightly greater than 0.35. Note the minor change in scale in between (b)–(d), (e), and (f), which however has no impact on the points made above.

It becomes clear that all features of the model are reproduced at least qualitatively by the data. The seams of interactions form a closed loop and the real and imaginary seam are connected by *two* CCI points lying symmetrically to the Q_g axis. The most pronounced deviation in between the model and the *ab initio* data results from the wiggles stemming from the change of basis with growing Q_g . Additionally, the model Hamiltonian from Sec. III F is only an expansion up to the linear term, and is thus expected to deviate from the *ab initio* data for larger values of Q_g/Q_u . Keeping both these points in mind, the agreement between the model and the *ab initio* data is astonishingly good.

We are now in a position to point to a possible reason for the deviation of the experimental from the calculated values at the equilibrium geometry. Looking at the real parts of the PES it is obvious that they repel each other with growing Q_u . Thus, if some vibrational modes along Q_u are excited, one would measure a higher electron affinity for the Σ^* and a lower for the Π^* resonance states than at the equilibrium geometry. This would nicely explain that our calculated energy for the Σ^* state apparently is too low and that for the Π^* state is too high. Using the model and the fitted parameters one even obtains energies of 2.85 and 1.32 eV, respectively, for the upper and lower states at $(Q_g, Q_u) = (0.0, \pm 20.0^\circ)$, which are very close to the experimental values (see above). But, on the one hand such high deflections in Q_u would afford highly excited vibrational modes, and on the

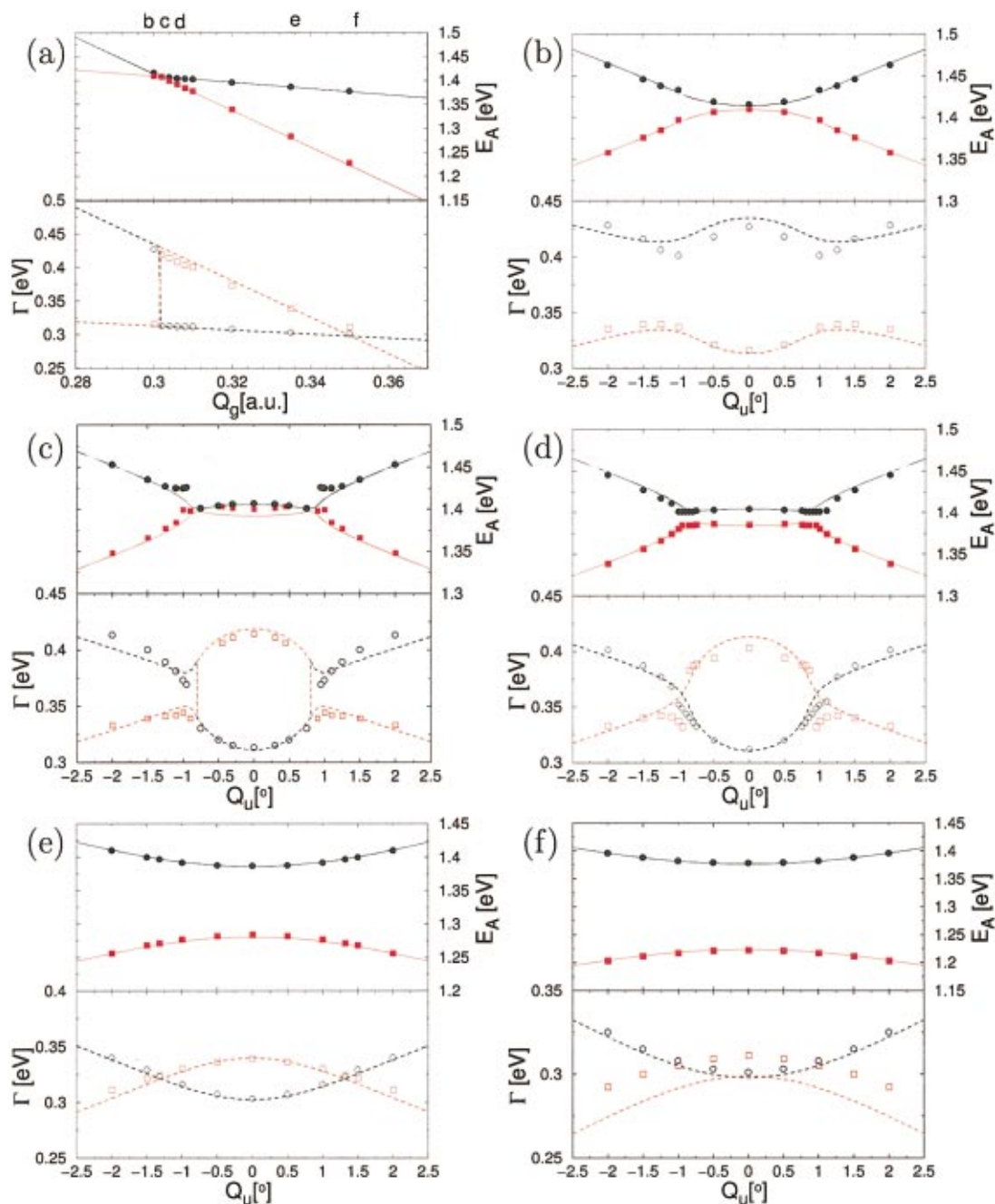


FIG. 7. (Color) Comparison of the *ab initio* data on the chloroethene anion with the complete linear model. Several cuts through the PES of the two resonance states are shown. Black circles were chosen for the *ab initio* data of the upper curve and red squares for the data of the lower curve. The lines represent the respective results obtained from the model; here, solid ones are negative electron attachment energies and dashed lines widths. (a) shows an enlarged view of Fig. 6 in the interaction region. The vertical dashed lines mark the locations of the cuts pictured in (b)–(f). These cuts are discussed in the text and lie at the following values of Q_g : (b) 0.3 a.u.; (c) 0.304 a.u.; (d) 0.308 a.u.; (e) 0.335 a.u.; and (f) 0.35 a.u. For the fit Q_u was converted to radians (see Table I), but the figures are pictured with Q_u in degrees.

other hand the fit to the model does not reproduce the Σ^* energy at $(Q_g, Q_u) = (0.0, 0.0^\circ)$ well (compare the value for E_1 in Table I and the one derived from Fig. 6 given above). Nevertheless, our explanation for the deviation at least holds qualitatively.

The goal to clearly reproduce the discontinuity in the imaginary parts of the PES unfortunately could not be achieved. Just at those points where it was expected to occur, i.e., near the CCI points, numerical problems occurred. Either additional stabilization points appeared in the η trajec-

tories, or on the contrary no stabilization points could be found at all for configurations in the (Q_g, Q_u) region of interest [see, e.g., Fig. 7(c)]. The numerical problems of the *ab initio* computations in the vicinity of these points can be interpreted as a clear hint that there is indeed a discontinuity.

Finally, let us have a look at the orbitals which get occupied by the additional electron. Normally, propagator calculations result in so-called Dyson orbitals, which can be viewed as correlated generalizations of molecular orbitals.⁶⁸ Since the Hamiltonian of the CAP/ $\Sigma^{(2)}$ method is complex,

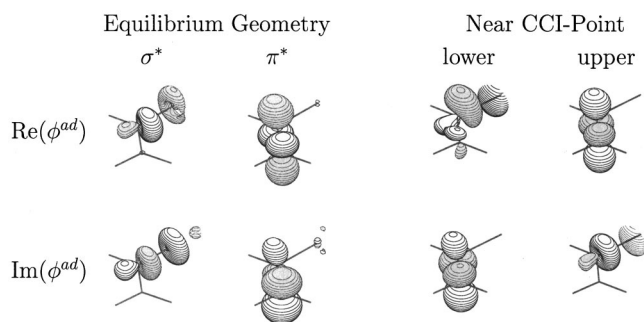


FIG. 8. Generalized molecular orbitals (see the text) calculated with CAP/ $\Sigma^{(2)}$ of the chloroethene anion at different points in nuclear coordinate space. The chlorine atom is located at the upper right corner. At the equilibrium geometry of neutral chloroethene, the orbitals are easily assigned to be of σ^* and π^* type. But, near the CCI points, the real part of the orbital with the lower energy (designated by “lower”) looks like a mixing of both orbital types, whereas the one with the higher energy (designated by “upper”) shows no obvious mixing. Additionally, the imaginary parts of the lower and upper orbitals have interchanged places.

we obtain complex continued Dyson orbitals here. We will call these orbitals generalized molecular orbitals (GMOs) for simplicity.

In Fig. 8 we show plots of the compact parts of the two GMOs, divided into their real and imaginary fractions. Note that the imaginary part is much more diffuse, i.e., the isodensity surfaces pictured in Fig. 8 are drawn at an approximately one order of magnitude smaller density for the imaginary part. Some interesting points can be seen immediately: At the equilibrium geometry, both the real and the imaginary part of the GMOs indeed look like typical σ^* and π^* orbitals, but the imaginary part has the opposite phase of the real part.

For the GMOs near the CCI points there are some profound changes. Whereas the real part of the upper (meaning higher in energy) orbital does not look significantly different from a π^* orbital, the real part of the lower orbital shows clear signs of a mixing of the π^* and the σ^* orbitals. Additionally, the imaginary parts of the two orbitals have interchanged places; a σ^* -like imaginary part pertains to the π^* -like real part and a clearly π^* -like imaginary part to the mixed, but mostly σ^* -like real part. This fits nicely with the picture obtained from the PES. The real parts of the PES have already crossed at this point in nuclear coordinate space, but not yet the imaginary parts. Hence, the real and imaginary parts of the orbitals correspond to the respective parts of the complex energy.

V. SUMMARY

In this paper we demonstrated that for PES of resonance states points of intersection can indeed occur—similar to conical intersections between PES of bound states—but additionally seams of intersections of the real and imaginary parts of the PES, respectively, arise. Since in many molecules two or more resonance states can be expected to approach each other in a limited region of nuclear coordinate space, these intersections of metastable states should be quite common and thus very relevant for many collision processes involving short-lived states.

We systematically constructed several model Hamiltonians describing the vibronic coupling of two resonance states, which also included the minimal model presented in Ref. 17. In particular, we introduced the “complete linear” model Hamiltonian which joins linear varying widths with a complex linear coupling term. This choice has the great advantage of still being analytically solvable and led to the interesting result of a closed loop of the intersection seams. Let us mention that the model Hamiltonians investigated here just include terms up to linear order and are thus only valid in the vicinity of the reference geometry. Further extensions of the model to increase the accuracy in regions further apart are straightforward—although more intricate models are not expected to possess explicit analytical solutions anymore.

The most interesting finding was the occurrence of exactly two intersection points, where both the real and the imaginary part of the energies coalesce, for all investigated model Hamiltonians. These two so-called complex conical intersection points provided the reason to term this complex analog of conical intersections “doubly intersecting complex energy surfaces,” or DICES for short. Another feature observed in all cases was a discontinuity occurring in the imaginary parts of the PES at the points where the seam of intersections of the real parts of the PES is located.

By calculating the PES of the resonance states of the chloroethene anion we also demonstrated that the complete linear model Hamiltonian reproduces the qualitative features of the PES quite nicely and also could be fitted reasonably well to the *ab initio* data. Due to numerical problems, it was not possible to reproduce the discontinuity occurring in the imaginary parts with the explicitly calculated data. Further work possibly will clarify how this could be achieved.

The results from the fit of the *ab initio* data of the resonance states of the chloroethene anion to the complete linear model Hamiltonian strongly suggest that DICES play a prominent role in the DEA process to chloroethene. Since this molecule is the prototype for a great number of other unsaturated halogenated compounds, the conclusion is evident that DICES are also responsible for the DEA process taking place in these compounds.

Our work shed considerable light on the details of the interaction of two resonance states through vibronic coupling. Molecular dynamics calculations which make use of this new description of intersections between metastable states are expected to give further interesting and illuminating results which finally will allow one to describe DEA processes and related phenomena more completely.

ACKNOWLEDGMENTS

Stimulating discussions with Dr. Björn Feuerbacher are acknowledged. Our thanks go to Maik Bittner for help with the figures. Finally, we thank the Deutsche Forschungsgemeinschaft for financial support.

¹M. Born and R. Oppenheimer, *Ann. Phys. (Leipzig)* **84**, 457 (1927).

²M. Born and K. Huang, *Dynamical Theory of Crystal Lattices* (Oxford University Press, New York, 1954).

³E. Teller, *J. Phys. Chem.* **41**, 109 (1937).

- ⁴H. Köppel, W. Domcke, and L. S. Cederbaum, *Adv. Chem. Phys.* **57**, 59 (1984).
- ⁵D. R. Yarkony, *J. Phys. Chem. A* **105**, 6277 (2001).
- ⁶*Adv. Chem. Phys., Vol. 124: The Role of Degenerate States in Chemistry*, edited by M. Baer and G. D. Billing (Wiley, NJ, 2002).
- ⁷*Conical Intersections: Electronic Structure, Dynamics, and Spectroscopy*, edited by W. Domcke, D. R. Yarkony, and H. Köppel (World Scientific, Singapore, 2003).
- ⁸*Electron-Molecule and Photon-Molecule Collisions*, edited by T. Rescigno, V. McKoy, and B. Schneider (Plenum, New York, 1979).
- ⁹M. A. Morrison, *Adv. At. Mol. Phys.* **24**, 51 (1987).
- ¹⁰C. L. Shoemaker and R. E. Wyatt, *Adv. Quantum Chem.* **14**, 169 (1981).
- ¹¹P. A. M. Dirac, *Z. Phys.* **44**, 585 (1927).
- ¹²V. Weisskopf, *Ann. Phys. (Leipzig)* **9**, 23 (1931).
- ¹³H. Feshbach, *Ann. Phys. (N.Y.)* **5**, 357 (1958).
- ¹⁴U. Fano, *Phys. Rev.* **124**, 1866 (1961).
- ¹⁵G. Gamow, *Z. Phys.* **51**, 204 (1928).
- ¹⁶A. J. F. Siegert, *Phys. Rev.* **56**, 750 (1939).
- ¹⁷H. Estrada, L. S. Cederbaum, and W. Domcke, *J. Chem. Phys.* **84**, 152 (1986).
- ¹⁸F. H. Mies, *Phys. Rev.* **175**, 164 (1968).
- ¹⁹A. U. Hazi, *J. Phys. B* **16**, L29 (1983).
- ²⁰A. Z. Devdariani, V. N. Ostrovskii, and Y. N. Sebyakin, *Sov. Phys. JETP* **49**, 266 (1979).
- ²¹R. S. Friedman, I. Podzielinski, L. S. Cederbaum, V. M. Ryaboy, and N. Moiseyev, *J. Phys. Chem. A* **106**, 4320 (2002).
- ²²L. S. Cederbaum, R. S. Friedman, V. M. Ryaboy, and N. Moiseyev, *Phys. Rev. Lett.* **90**, 013001 (2002).
- ²³S. L. Lunt, D. Field, S. V. Hoffmann, R. J. Gulley, and J.-P. Ziesel, *J. Phys. B* **32**, 2707 (1999).
- ²⁴A. Modelli and M. Venuti, *J. Phys. Chem. A* **105**, 5836 (2001).
- ²⁵H. Abdoul-Carime, M. A. Huels, F. Brüning, E. Illenberger, and L. Sanche, *J. Chem. Phys.* **113**, 2517 (2000).
- ²⁶T. Sommerfeld, *ChemPhysChem* **2**, 677 (2001).
- ²⁷T. F. O'Malley, *Adv. At. Mol. Phys.* **7**, 223 (1971).
- ²⁸C. J. Ballhausen and A. E. Hansen, *Annu. Rev. Phys. Chem.* **23**, 15 (1972).
- ²⁹C. A. Mead and D. G. Truhlar, *J. Chem. Phys.* **77**, 6090 (1982).
- ³⁰C. A. Mead, *J. Chem. Phys.* **78**, 807 (1983).
- ³¹T. Pacher, L. S. Cederbaum, and H. Köppel, *Adv. Chem. Phys.* **84**, 293 (1993).
- ³²A. U. Hazi, *J. Phys. B* **11**, L259 (1978).
- ³³*Electron-Atom and Electron-Molecule Collisions*, edited by J. Hinze (Plenum, New York, 1983).
- ³⁴J. R. Taylor, *Scattering Theory* (Wiley, New York, 1972).
- ³⁵A. U. Hazi and H. S. Taylor, *Phys. Rev. A* **1**, 1109 (1970).
- ³⁶N. Moiseyev, *Phys. Rep.* **302**, 211 (1998).
- ³⁷G. Jolicard and E. J. Austin, *Chem. Phys. Lett.* **121**, 106 (1985).
- ³⁸U. V. Riss and H.-D. Meyer, *J. Phys. B* **26**, 4503 (1993).
- ³⁹T. Sommerfeld, U. V. Riss, H.-D. Meyer, L. S. Cederbaum, B. Engels, and H. U. Suter, *J. Phys. B* **31**, 4107 (1998).
- ⁴⁰S. Feuerbacher, T. Sommerfeld, R. Santra, and L. S. Cederbaum, *J. Chem. Phys.* **118**, 6188 (2003).
- ⁴¹P. G. Burke, in *Electron-Molecule Scattering and Photoionization: An R-Matrix Approach*, edited by K. A. Berrington (Plenum, New York, 1993).
- ⁴²C. Winstead, V. McKoy, and A. A. Noyes, *Adv. Chem. Phys.* **96**, 103 (1996).
- ⁴³T. Sommerfeld, *Phys. Chem. Chem. Phys.* **4**, 2511 (2002).
- ⁴⁴W. Domcke, *Phys. Rep.* **208**, 97 (1991).
- ⁴⁵D. D. Clarke and C. A. Coulson, *J. Chem. Soc. A* **1**, 169 (1969).
- ⁴⁶J. K. Olthoff, J. A. Tossell, and J. H. Moore, *J. Chem. Phys.* **83**, 5627 (1985).
- ⁴⁷J. A. Stockdale and G. S. Hurst, *J. Chem. Phys.* **41**, 255 (1964).
- ⁴⁸K. L. Stricklett, S. C. Chu, and P. D. Burrow, *Chem. Phys. Lett.* **131**, 279 (1986).
- ⁴⁹P. D. Burrow, A. Modelli, N. S. Chiu, and K. D. Jordan, *Chem. Phys. Lett.* **82**, 270 (1981).
- ⁵⁰R. Kaufel, E. Illenberger, and H. Baumgärtel, *Chem. Phys. Lett.* **106**, 342 (1984).
- ⁵¹E. Rivera and R. H. Schuler, *J. Phys. Chem.* **87**, 3966 (1983).
- ⁵²L. G. Christophorou, *Electron-Molecule Collisions and their Applications* (Academic, New York, 1984), Vol. 2.
- ⁵³M. Born, S. Ingemann, and N. M. M. Nibbering, *Mass Spectrom. Rev.* **16**, 181 (1997).
- ⁵⁴E. Illenberger, *Adv. Ser. Phys. Chem.* **10B**, 1063 (2000).
- ⁵⁵L. G. Christophorou, *Adv. At. Mol. Phys.* **44**, 155 (2001).
- ⁵⁶R. Yoshimura and T. Tada, *Chem. Phys. Lett.* **222**, 626 (1994).
- ⁵⁷T. Skalický, C. Chollet, N. Pasquier, and M. Allan, *Phys. Chem. Chem. Phys.* **4**, 3583 (2002).
- ⁵⁸M. W. Schmidt, J. A. Boatz, K. K. Baldrige, S. Koseki, M. S. Gordon, S. T. Elbert, and B. Lam, *QCPE Bull.* **7**, 115 (1987).
- ⁵⁹MOLCAS VERSION 5, Authors: K. Andersson, M. Barysz, A. Bernhardsson *et al.*, University of Lund, Sweden (2001).
- ⁶⁰A. L. Fetter and J. D. Walecka, *Quantum Theory of Many-Particle Systems* (McGraw-Hill, New York, 1971).
- ⁶¹R. Santra and L. S. Cederbaum, *J. Chem. Phys.* **117**, 5511 (2002).
- ⁶²J. Schirmer, L. S. Cederbaum, and O. Walter, *Phys. Rev. A* **28**, 1237 (1983).
- ⁶³W. von Niessen, J. Schirmer, and L. S. Cederbaum, *Comput. Phys. Rep.* **1**, 57 (1984).
- ⁶⁴N. F. Lane, *Rev. Mod. Phys.* **52**, 29 (1980).
- ⁶⁵L. Sanche and G. J. Schulz, *Phys. Rev. A* **5**, 1672 (1972).
- ⁶⁶R. Santra, L. S. Cederbaum, and H.-D. Meyer, *Chem. Phys. Lett.* **303**, 413 (1999).
- ⁶⁷T. H. Dunning, Jr. and P. J. Hay, in *Methods of Electronic Structure Theory*, edited by H. F. S. III (Plenum, New York, 1977).
- ⁶⁸R. McWeeny, *Methods of Molecular Quantum Mechanics* (Academic, London, 1992).